

Solar Sail Deployment Dynamics

Behrad Vatankhahghadim¹ and Christopher J. Damaren¹

¹*Institute for Aerospace Studies, University of Toronto, {behrad.vatankhahghadim@mail, damaren@utias}.utoronto.ca*

ABSTRACT — *The deployment dynamics of a solar sail consisting of four flexible booms and four membrane quadrants are studied. First, previous work on modelling a portion of the system (only one membrane quadrant attached to two axially-moving booms) using time-varying quasi-modal expansion is extended to be applicable to the complete system. This is achieved via “lifting” the quadrant-level matrices into system-level forms by partitioning them (based on the generalized coordinates of each of the two booms or the membrane in-between, to which each block should correspond) and placing each block into a large matrix using an appropriate mapping table (with the remaining blocks left as zero matrices). Once all matrices are converted to system-level forms, the equations of motion from previous work readily apply to the complete system (now involving all of the booms’ and membranes’ generalized coordinates). Modal analysis is performed on a constant-length sail to validate the basic foundations of the model by comparing the results to the finite elements-based ones from literature. Deployment simulation results are presented, and numerical parameter studies are performed using the eigenvalues of the system (recast into first-order form).*

1 Introduction

Translating continua of constant or time-varying length find applications in many areas of engineering, such as magnetic tapes, elevator cables, robotic arms, paper industry, and spacecraft antennae. Surveys of some of the early works in such areas were presented in [1, 2], and more recent efforts were reviewed in [3]. In the context of spacecraft, deployment was examined in [4, 5, 6, 7], among others. More generally, studies on axially-translating strings, considered to be among the simplest of translating continua that lead to second-order equations, can be traced back to [8, 9, 10]. Transverse vibration of axially-translating beams, described by fourth-order systems, was studied in [11, 12, 13, 14, 15, 16], among others, in which a “quasi-modal expansion” using the eigenfunctions of a cantilevered beam was used to express the transverse deflections (similarly to [17, 18, 19] for spacecraft applications). In addition, out-of-plane dynamics of translating membranes were examined in [20, 21, 22], where one-dimensional motion between two supports of fixed distance was considered, in contrast to the two-dimensional and variable-length problem of interest in this work that also features coupling between beams and membranes.

Focusing on the dynamics of coupled multibody systems, most relevant past works include [23, 24] (assuming constant boom length) and [25] (accounting for temporal variations). These references also make use of the aforementioned quasi-modal approach, but to ensure compatibility of displacements at the points of attachments of their models’ booms and solar panels (treated as beams and membranes), they express the deflections of the latter in terms of those of the former. Making use of a similar formulation, out-of-plane deflections of a solar sail quadrant (consisting of two axially-translating booms with a membrane in-between) was examined in [26], in which upon deriving the equations of motion, analytic expressions for the rate of change of vibration energy (resembling those in [27, 15] for deploying beams) were also obtained.

Heavily numerical approaches (using Multi-Particle Model and Absolute Nodal Coordinate Formulation, for example) for studying the deployment dynamics of solar sails, namely IKAROS, were used in several recent resources, such as in [28], replacing each finite element with masses, springs, and dampers; and in [29, 30], using a global coordinate system to arrive at a constant mass matrix. Abandoning simple analytical models, [31] developed a numerical method in a geometrically nonlinear Finite Element Method (FEM) framework, and proposed elements

with variable length, mass, and moment of inertia for a more realistic simulation of deployment of IKAROS. Examples of earlier works on translating beams and membranes that also made use of FEM include [32, 33] and [20, 21], respectively.

A natural and important question that arises in the context of deployable structures is that of stability. Translating continua of varying length could be classified as non-conservative gyroscopic systems [32]. For such systems, static methods such as those seeking the appearance of non-trivial equilibria may yield results that are inconsistent with the more reliable ones furnished by the kinetic (vibration) methods [34]. In the past, stability of translating materials has been studied by examining the transverse displacements' boundedness, such as in [35, 33, 36, 3], as well as from an energy viewpoint, such as in [10, 37, 27, 3]. In [26], it was shown that the transverse vibration energy of the hybrid beam-membrane system of a solar sail monotonically decreases and increases during deployment and retraction, respectively. Similarly to the observations reported in [27, 15], however, this conclusion, elegant as it is, does not guarantee boundedness of displacements during extension (which, in fact, behaves unlike vibration energy and increases).

A primary contribution of this manuscript is to build upon [26] and numerically investigate the possibility of divergence and flutter using a kinetic approach, and study the effects of pretension and deployment rate on the onset of such phenomena. Whereas the formulation of that work primarily focused on a single sail quadrant (a triangular membrane attached to deploying booms), the present document provides more details on a complete and more realistic model of a solar sail, namely one with four axially-translating beams, with four thin membrane quadrants attached in-between. New stability results pertinent to the complete sail's behaviour are also presented. Upon validating the constant-length results against those in [38] via modal analysis (as deployment results are not available for this model), dynamic simulations are performed using a plausible extension/retraction profile. In contrast to the energy-based approach of [26] that yielded simple analytic expressions for assessing boundedness of vibration energy (a measure of dynamic stability in the sense of energy suppression), the present work adopts the kinetic vibration approach that yields a quadratic eigenvalue problem. Numerical eigenvalue studies are then performed, and the results seem to suggest the existence of instability regions in terms of amplitude growth (an aspect that was not accounted for by the energy approach of [26]), for certain combinations of extension rate and sail tension.

The organization of this manuscript is as follows: Section 2 describes the model of interest and some simplifying assumptions made to make the problem tractable. The discretization approach of and the resulting discretized equations of motion (for a quadrant) in [26] are reviewed in Section 3 (and Appendix A), and more details are provided on extending these derivations to a complete sail and a reformulation of the problem to enable numerical stability analyses. Simulation results related to static (for validation) and dynamics sails are presented in Section 4, along with those on the sail's deployment stability.

2 Model Description and Assumptions

A square solar sail model as shown in Fig. 1 is considered. Only out-of-plane deflections of the sail quadrants and their support booms are considered in the present manuscript, and accounting for the in-plane deflections (and the possibility of wrinkling) are left as part of future work. Uniform thin membranes (with no bending stiffness) and Euler-Bernoulli beams (with no axial extensibility) are used to model the sail and the booms, respectively. Consistent with [26], a sliding-type deployment is assumed, with the free edge remaining straight and at 45° to the booms at all times. This assumption is admittedly unrealistic, especially considering the many folds to which packaged sails are subjected, but it is a key assumption to render the problem tractable, and is believed to capture the main behaviour of the system (upon which future higher fidelity studies can build). The resulting velocity distribution is [26]:

$$v_x = \frac{\dot{L}}{2} \left(1 + \frac{x_{ab} - y_{ab}}{x_{ab} + y_{ab}} \right), \quad v_y = \frac{\dot{L}}{2} \left(1 - \frac{x_{ab} - y_{ab}}{x_{ab} + y_{ab}} \right) \quad (1)$$

where \dot{L} is the constant deployment rate of the booms, v_x and v_y are the components of the mass elements' in-plane deployment velocity, in the reference frame attached to Quadrant Q_{ab} .

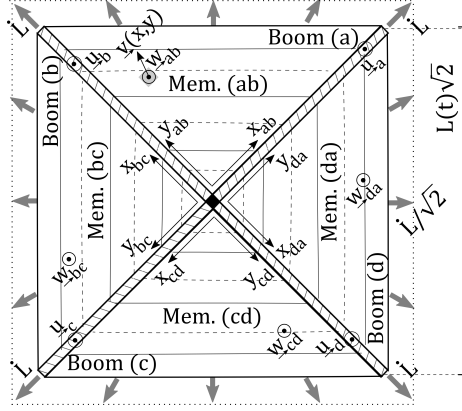


Fig. 1: Model of Deploying Solar Sail: Booms (a), (b), (c), and (d); and Membrane Quadrants (ab), (bc), (cd), (da) with Straight Free Edges

The membrane quadrants are taken to be under linearly increasing (towards the boom tips) forces per unit length, namely normal N_{xx} and N_{yy} and shear N_{xy} , provided by the booms. This results in compressive axial loads, P , on the latter. The corresponding expressions related to Membrane (ab) and Boom (a), for example, are [26]:

$$N_{xx} = N_{yy} = -N_{xy} = \frac{\bar{\sigma}h}{L_0}(x_{ab} + y_{ab}) \quad , \quad P_a = -\frac{\bar{\sigma}A}{L_0}x_{ab} \quad (2)$$

where $\bar{\sigma}$ is the maximum prestress at the tips, h is the uniform membrane thickness, and A and $L(t)$ are the booms' uniform cross-sectional area and time-varying length, respectively, with $L_0 = L(0)$.

3 Discretized Equations of Motion

The quasi-modal approach with time-varying basis functions used by [5, 25, 13, 19, 15] is adopted. The out-of-plane deflections of the booms and the membrane (superimposed over the booms' deflections as was done in [24], for constant length, and in [25], for deployment) are expanded, using n_B and n_M modes, respectively, as [26]:

$$u_a(x_{ab}, t) = \mathbf{p}_a^\top(t) \Psi_a(x_{ab}, t) \quad , \quad u_b(y_{ab}, t) = \mathbf{p}_b^\top(t) \Psi_b(y_{ab}, t) \quad (3a)$$

$$w_{ab}(x_{ab}, y_{ab}, t) = u_a(x_{ab}, t) + u_b(y_{ab}, t) + \mathbf{q}_{ab}^\top(t) \Phi_{ab}(x_{ab}, y_{ab}, t) \quad (3b)$$

where $\mathbf{p}_a \in \mathbb{R}^{n_B}$, $\mathbf{p}_b \in \mathbb{R}^{n_B}$, and $\mathbf{q}_{ab} \in \mathbb{R}^{n_M}$ are the generalized coordinates of Boom (a), Boom (b) and Membrane (ab), respectively. The time-varying components of Ψ_a , Ψ_b , and Φ_{ab} , which are the eigenfunctions of a cantilevered beam and an all-edges clamped membrane, depend on $x/L(t)$ and/or $y/L(t)$.

3.1 Quadrant-Level Equations of Motion

Using the expansions in Eq. (3) and the standard Lagrangian mechanics-based formulation involving the system's energy expressions, the following discretized equations of motion (with the required matrices in Appendix A) for a single sail quadrant consisting of Membrane (ab) attached to Booms (a) and (b) were obtained in [26]:

$$\left[\tilde{\mathbf{M}}_M + \tilde{\mathbf{M}}_B \right] \ddot{\tilde{\mathbf{q}}} + \left[(\dot{\tilde{\mathbf{M}}}_M + \dot{\tilde{\mathbf{M}}}_B) + (\tilde{\mathbf{G}}_M - \tilde{\mathbf{G}}_M^\top) + (\tilde{\mathbf{G}}_B - \tilde{\mathbf{G}}_B^\top) \right] \dot{\tilde{\mathbf{q}}} + \left[(\dot{\tilde{\mathbf{G}}}_M + \dot{\tilde{\mathbf{G}}}_B) + (\Delta\tilde{\mathbf{K}}_M + \Delta\tilde{\mathbf{K}}_B) \right] \tilde{\mathbf{q}} = \mathbf{0} \quad (4)$$

where $\tilde{\mathbf{q}} \triangleq [\mathbf{p}_a^\top \quad \mathbf{p}_b^\top \quad \mathbf{q}_{ab}^\top]^\top$ contains all of the Q_{ab} quadrant's generalized coordinates, and $\Delta\tilde{\mathbf{K}}_M \triangleq \mathbf{K}_{M,U} - \mathbf{K}_{M,T}$ and $\Delta\tilde{\mathbf{K}}_B \triangleq \mathbf{K}_{B,U} - \mathbf{K}_{B,T}$. The quadrant-level matrices denoted by a tilde are of dimensions $\tilde{n} \times \tilde{n}$ with $\tilde{n} = 2n_B + n_M$, and are constructed via spatial integration of some functions of Ψ and Φ , as provided in Appendix A. Note that the boom-related matrices (with the subscript 'B') have zero partitions corresponding to the membrane's generalized coordinates: for example, $\tilde{\mathbf{M}}_B \triangleq \text{blockdiag}\{\mathbf{M}_B, \mathbf{M}_B, \mathbf{0}_{n_M \times n_M}\}$, where the inner blocks (without a tilde, for they relate to the booms only) are the ones presented in Appendix A.

3.2 System-Level Equations of Motion

Recognizing a need for completeness in modelling and simulation, the present work first provides more details on how the formulation of Subsection 3.1 can be extended to apply to a complete four-quadrant sail. The methodology to be presented can also be modified accordingly for different geometries with other numbers of booms and membranes. To achieve this extension, the quadrant-level matrices are “lifted” into system-level forms that correspond to the system-level collection of *all* generalized coordinates, $\bar{\mathbf{q}} \triangleq [\mathbf{p}_a^\top \mathbf{p}_b^\top \mathbf{p}_c^\top \mathbf{p}_d^\top \mathbf{q}_{ab}^\top \mathbf{q}_{bc}^\top \mathbf{q}_{cd}^\top \mathbf{q}_{da}^\top]^\top$.

First, each of the quadrant-level matrices are partitioned into nine submatrices (for example $\tilde{\mathbf{M}}_{M,ab,ij}$ with $i, j \in \{1, 2, 3\}$) that correspond to \mathbf{p}_a , \mathbf{p}_b , and \mathbf{q}_{ab} , as follows:

$$\tilde{\mathbf{M}}_{M,ab} = \begin{bmatrix} \tilde{\mathbf{M}}_{M,ab,11} & \tilde{\mathbf{M}}_{M,ab,12} & \tilde{\mathbf{M}}_{M,ab,13} \\ \tilde{\mathbf{M}}_{M,ab,21} & \tilde{\mathbf{M}}_{M,ab,22} & \tilde{\mathbf{M}}_{M,ab,23} \\ \tilde{\mathbf{M}}_{M,ab,31} & \tilde{\mathbf{M}}_{M,ab,32} & \tilde{\mathbf{M}}_{M,ab,33} \end{bmatrix} \begin{matrix} n_B \\ n_B \\ n_M \end{matrix} \quad (5)$$

The system-level mass matrix corresponding to the \mathbf{Q}_{ab} quadrant’s membrane, denoted by $\bar{\mathbf{M}}_{M,ab}$ and of dimensions $\bar{n} \times \bar{n}$ with $\bar{n} = 4n_B + 4n_M$, can be partitioned into 64 blocks, namely $\bar{\mathbf{M}}_{M,ab,pq}$ with $p, q \in \{1, \dots, 8\}$. Of these 64 blocks, nine are replaced by $\tilde{\mathbf{M}}_{M,ab,ij}$ in Eq. (5), and the rest are all zero matrices of appropriate dimensions. Summarized in Tab. 1 is the mapping between the indices of the quadrant-level matrices and those of the system-level matrices. For example, the $\tilde{\mathbf{M}}_{M,ab,23}$ block of the quadrant-level $\tilde{\mathbf{M}}_{M,ab}$ replaces the $\bar{\mathbf{M}}_{M,ab,25}$ block of the system-level $\bar{\mathbf{M}}_{M,ab}$, because the generalized coordinates of Boom (b) and Quadrant (ab), the second and third blocks of $\bar{\mathbf{q}}$ which correspond to the (2,3) block of the relevant quadrant-level matrices, are now located in second and fifth blocks of the complete coordinates gathered in $\bar{\mathbf{q}}$.

Lastly, after all of the matrices in Eq. (4) for all four quadrants are lifted into their system-level form using the above procedure and the mapping in Tab. 1, the overall system matrices are computed by simple addition. For example, the membranes’ total mass matrix is given by $\bar{\mathbf{M}}_M = \bar{\mathbf{M}}_{M,ab} + \bar{\mathbf{M}}_{M,bc} + \bar{\mathbf{M}}_{M,cd} + \bar{\mathbf{M}}_{M,da}$, while that of the booms is $\bar{\mathbf{M}}_B = \bar{\mathbf{M}}_{B,ab} + \bar{\mathbf{M}}_{B,bc} + \bar{\mathbf{M}}_{B,cd} + \bar{\mathbf{M}}_{B,da}$, and so on for all matrices. The resulting system matrices, replacing their quadrant-level counterparts in Eq. (4), along with the system-level coordinates in $\bar{\mathbf{q}}$ and their time derivatives, describe the complete system’s motion:

$$\underbrace{\left[\bar{\mathbf{M}}_M + \bar{\mathbf{M}}_B \right]}_{\bar{\mathbf{M}}_{eq}} \ddot{\bar{\mathbf{q}}} + \underbrace{\left[(\dot{\bar{\mathbf{M}}}_M + \dot{\bar{\mathbf{M}}}_B) + (\bar{\mathbf{G}}_M - \bar{\mathbf{G}}_M^\top) + (\bar{\mathbf{G}}_B - \bar{\mathbf{G}}_B^\top) \right]}_{\bar{\mathbf{G}}_{eq}} \dot{\bar{\mathbf{q}}} + \underbrace{\left[(\ddot{\bar{\mathbf{G}}}_M + \ddot{\bar{\mathbf{G}}}_B) + (\Delta\bar{\mathbf{K}}_M + \Delta\bar{\mathbf{K}}_B) \right]}_{\bar{\mathbf{K}}_{eq}} \bar{\mathbf{q}} = \mathbf{0} \quad (6)$$

where $\Delta\bar{\mathbf{K}}_M \triangleq \bar{\mathbf{K}}_{M,U} - \bar{\mathbf{K}}_{M,T}$ and $\Delta\bar{\mathbf{K}}_B \triangleq \bar{\mathbf{K}}_{B,U} - \bar{\mathbf{K}}_{B,T}$. For simplicity, new system-level matrices $\bar{\mathbf{M}}_{eq}$, $\bar{\mathbf{G}}_{eq}$, and $\bar{\mathbf{K}}_{eq}$ are defined to denote the “equivalent” mass, gyricity/damping, and stiffness matrices. However, the reader is cautioned that they do not, in general, possess the same symmetry and definiteness properties that are typically associated with these terms in mechanical systems. For example, the “equivalent stiffness” matrix is not necessarily positive-definite.

3.3 Quadratic Eigenvalue Problem

The kinetic vibration approach (so-termed in [34]) to stability is adopted in this work. Upon assuming solutions of exponential form (as functions of time), the system in Eq. (6) leads to the following quadratic eigenvalue problem:

$$\bar{\mathbf{M}}_{eq}\ddot{\bar{\mathbf{q}}} + \bar{\mathbf{G}}_{eq}\dot{\bar{\mathbf{q}}} + \bar{\mathbf{K}}_{eq}\bar{\mathbf{q}} = \mathbf{0} \Rightarrow \det\left(\lambda^2\bar{\mathbf{M}}_{eq} + \lambda\bar{\mathbf{G}}_{eq} + \bar{\mathbf{K}}_{eq}\right) = 0 \quad (7)$$

Quadrant	\mathbf{Q}_{ab}			\mathbf{Q}_{bc}			\mathbf{Q}_{cd}			\mathbf{Q}_{da}		
Quadrant-Level (i, j)	1	2	3	1	2	3	1	2	3	1	2	3
System-Level (p, q)	1	2	5	2	3	6	3	4	7	4	1	8

Tab. 1: Mapping between Block Indices of the Partitioned Quadrant-Level and System-Level Matrices

which leads to $2\bar{n} = 8n_B + 8n_M$ eigenvalues. Problems of this type were considered in detail in [39], and algorithms (claimed to be superior for certain problems) are available, for example in [40], that attempt to solve them by avoiding a reformulation into first-order form. However, to allow for a comparison against the results of [33] (for a single deploying beam), and consistent with [20, 22] (focusing on translating membranes), the second-order system of Eq. (6) is first recast into a first-order form, leading to the following generalized eigenvalue problem:

$$\underbrace{\begin{bmatrix} \bar{M}_{\text{eq}} & \mathbf{0} \\ \mathbf{0} & \bar{M}_{\text{eq}} \end{bmatrix}}_{\bar{\mathbb{A}}} \underbrace{\begin{bmatrix} \ddot{\bar{q}} \\ \dot{\bar{q}} \end{bmatrix}}_{\dot{\bar{x}}} + \underbrace{\begin{bmatrix} \bar{G}_{\text{eq}} & \bar{K}_{\text{eq}} \\ -\bar{M}_{\text{eq}} & \mathbf{0} \end{bmatrix}}_{\bar{\mathbb{B}}} \underbrace{\begin{bmatrix} \dot{\bar{q}} \\ \bar{q} \end{bmatrix}}_{\bar{x}} = \mathbf{0} \Rightarrow \det(\lambda \bar{\mathbb{A}} + \bar{\mathbb{B}}) = 0 \quad (8)$$

where each pair of eigenvalues are associated with a different vibration mode. The resulting eigenvalues were confirmed to match closely with those obtained using the algorithm provided by [40]. For simplicity of implementation, however, and to allow for the consistent determination and sorting of the eigenvalues (via the *eigenshuffle()* function available for MATLAB), further manipulation into the following standard eigenvalue problem was performed:

$$\dot{\bar{x}} = \underbrace{\begin{bmatrix} -\bar{M}_{\text{eq}}^{-1} \bar{G}_{\text{eq}} & -\bar{M}_{\text{eq}}^{-1} \bar{K}_{\text{eq}} \\ \mathbf{1} & \mathbf{0} \end{bmatrix}}_{\bar{\mathbb{C}}} \bar{x} \Rightarrow \det(\lambda \mathbf{1} - \bar{\mathbb{C}}) = 0 \quad (9)$$

where invertibility of the equivalent mass matrix is assumed.

Lastly, it is worth emphasizing that, despite having formulated an eigenvalue problem for the system of interest, the matrices associated with a given deployment scenario are time-varying and they do not, in general, offer clear implications about stability. In other words, the eigenvalues are not “natural frequencies” of the system owing to its time-varying nature. In terms of past works on stability analysis, the parameter variations in [33], for example, were interpreted in two ways [41]: keeping the boom length fixed and varying the rate (treating each simulation case as an independent deployment scenario), and vice versa (changing length over time during a given deployment scenario). It is the former interpretation that is adopted here (and was also used in [42] to study the stability of deploying plates of varying length) for it is more meaningful, but the resulting critical values would be the same with both viewpoints [41]. In addition to varying the deployment rate, the results in Section 4.3 also shed some light on the effects of different values of membrane pretension and mass density.

4 Results and Discussion

Numerical simulations are performed using some of the solar sail parameters considered in [43], unless otherwise stated, including $\rho = 2.32 \times 10^{-2}$ kg/m, $EI = 4.62 \times 10^3$ N·m², and $A = 3.22 \times 10^{-5}$ m² for all of the booms; and $\mu = 1.39 \times 10^{-2}$ kg/m² (or $\mu = 1.39 \times 10^{-1}$ kg/m² for heavier membranes) and $h = 1 \times 10^{-5}$ m for all of the membrane quadrants. The constant-length and deploying sail simulations of Subsections 4.1 and 4.2 are based on Eq. (6) (and the modal properties associated with the equivalent system matrices involved in it), while the stability results in Subsection 4.3 are obtained using Eq. (9). All dynamic simulations make use of the Newmark-Beta algorithm of [44] with $\beta = 1/2$ and a step-size of $\Delta t = 0.0001$ s. The numbers of modes used for each boom and membrane quadrant in the expansions described in Section 3 are set to $n_B = 4$ and $n_M = 16$, respectively.

4.1 Validation

Before studying deployment, validation of the basics of the modelling and simulation using past literature is in order. To this end, the mode shapes and frequencies of the entire sail, after full deployment into a 100 m × 100 m square shape with a pretension profile given by $\bar{\sigma} = 100$ kPa, are compared against those obtained in [38] using the different FEM-based formulation. The first 6 modal frequencies (obtained upon neglecting axial tension imposed on the booms in Eq. (2), consistent with [38], and using the same parameters, in turn based on those in [43]) are listed in Tab. 2. They show less than 3% discrepancy compared with those reported in [38], and the associated mode

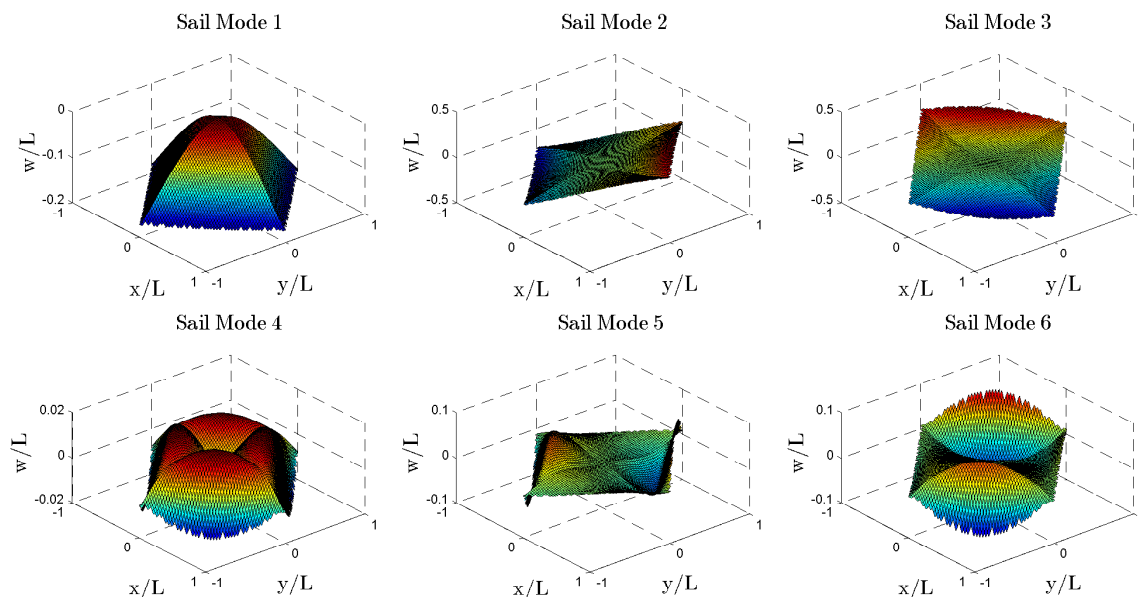


Fig. 2: First 6 Modes of Solar Sail with Boom Length $L = 50\sqrt{2}$ m (for Comparison against Figure 6 in [38])

shapes presented in Fig. 2 resemble those in [38]. As expected, the complete sail has additional symmetric/anti-symmetric modes that would not appear in the single sail quadrant that was the primary focus of [26].

4.2 Dynamic Simulation

First, a symmetric deployment case is considered as a sanity check. The initial conditions (ICs) of two opposite booms, namely Booms (a) and (c), assumed to be initially perturbed by equal amounts, are set to $\mathbf{p}_a(0) = \mathbf{p}_c(0) = [1 \ 0 \ 0 \ 0]^T / L(0)$ and $\dot{\mathbf{p}}_a(0) = \dot{\mathbf{p}}_c(0) = \mathbf{0}_{4 \times 1}$, while those of Booms (b) and (d) and the membrane quadrants (whose deflections relative to the booms are represented by $\mathbf{q}(0)$) are set to zero (with zero rates). A smaller tension (compared to Subsection 4.1) of $\bar{\sigma} = 2$ kPa is used, now with the booms' compression in Eq. (2) also modelled, and their length varied using a realistic profile that features initial acceleration and final deceleration: $L(t) = 10 + 2.5[1 - \cos(\pi t/t_f)]$ m, where $t_f = 15$ s specifies how long extension from 10 m to 15 m of the sail is expected to last. Snapshots of the motion sequence are provided in Fig. (3) and they confirm that symmetry is maintained throughout deployment.

To focus on how deflections propagate from a single corner on the sail to other areas, the results shown in Figs. 4a and 4b have only their Boom (a) initially deflected by $\mathbf{p}_a(0) = [1 \ 0 \ 0 \ 0]^T / L(0)$ and $\dot{\mathbf{p}}_a(0) = \dot{\mathbf{p}}_c(0) = \mathbf{0}_{4 \times 1}$, and the rest of the initial conditions are set to zero. Both sets of results use the same sail tension as that in Fig. 3, namely $\bar{\sigma} = 2$ kPa, and they differ from each other in terms of their membrane mass: the sail in Fig. 4a has the same membrane mass density as previous simulations, namely $\mu = 1.39 \times 10^{-2}$ kg/m², but that in Fig. 4b uses an order of magnitude heavier sail membrane with $\mu = 1.39 \times 10^{-1}$ kg/m². All the other parameters are kept the same as those in the previous simulations, and the extension profile used for Fig. (3) is utilized. The aim is to assess the relative effect of membrane quadrants on the booms, and to help facilitate this, provided in Fig. 4c are the tip deflections of Boom (c), the furthest corner from the point of initial displacement. The results suggest the presence of a heavier membrane entails more pronounced propagation of deflections throughout the sail.

Modal Frequency	ω_1	ω_2	ω_3	ω_4	ω_5	ω_6
Using FEM [38] (rad/s)	0.05180	0.20848	0.20848	0.30520	0.36781	0.36781
Present Method (rad/s)	0.05328	0.20954	0.20954	0.31002	0.37091	0.37091

Tab. 2: Comparison of the First 6 Modal Frequencies (for Fully-Deployed Sail) Obtained Using the Present Approach vs. FEM in [38]

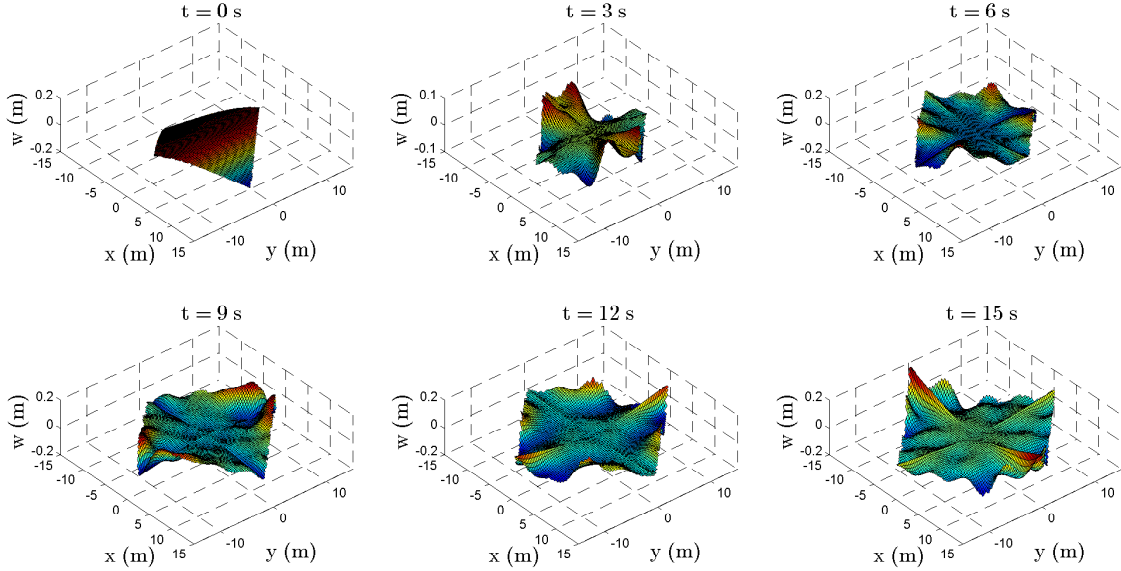


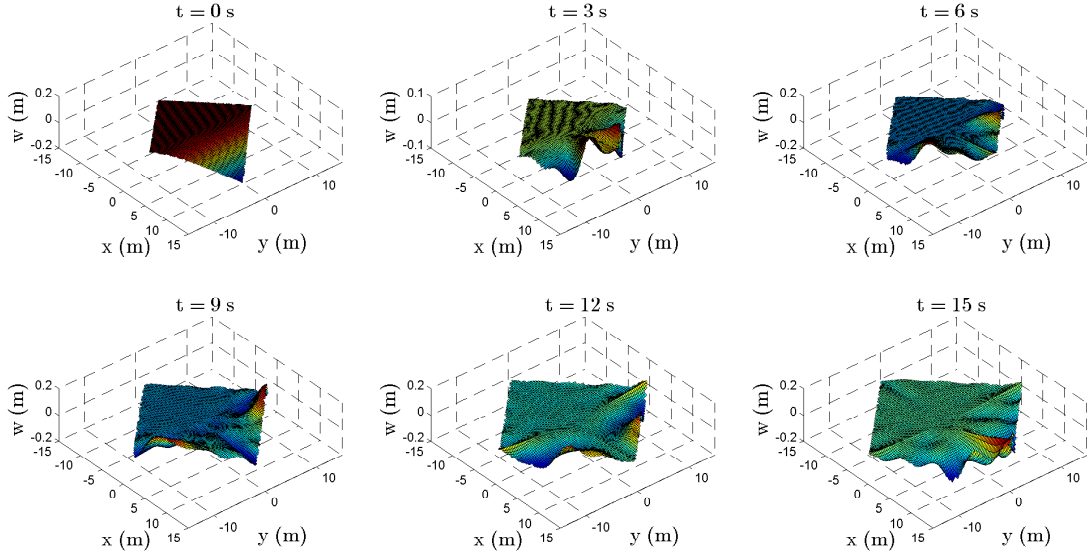
Fig. 3: Snapshots of Simulated Sail Deployment Process with Symmetric ICs (from $L(0) = 10$ m to $L(t_f) = 15$ m in 15 s)

4.3 Stability Analysis

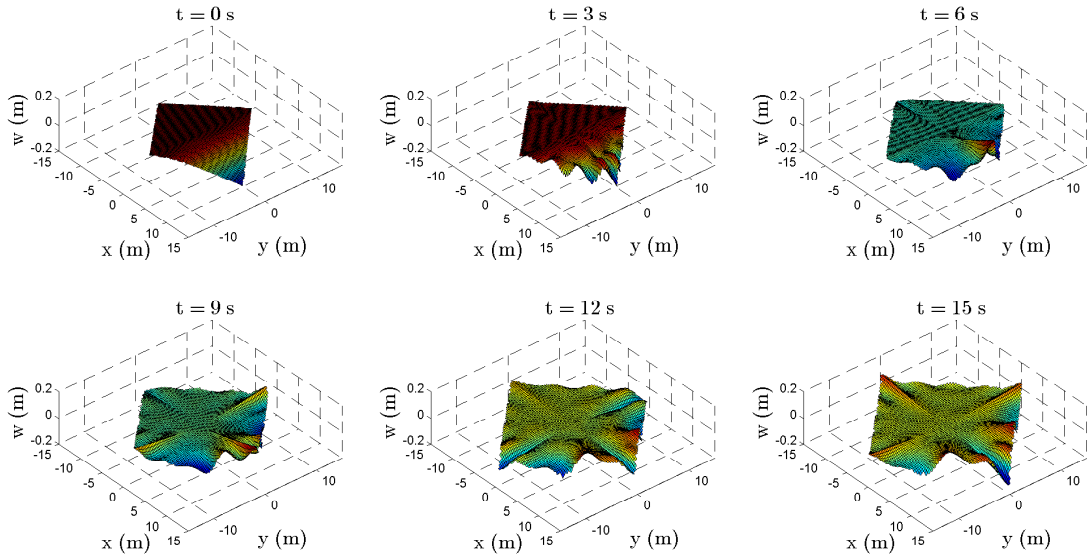
The effects of each parameter of interest, namely deployment rate and pretension, are studied as described in Subsection 3.3, upon fixing the boom length and performing a “frozen” eigenvalue analysis. Given that an eigenvalue with a positive real part implies instability, the resulting eigenvalues are sorted in descending order based on their real parts. Shown in Fig. 5 are the changes in the real and imaginary parts of the first 3 distinct eigenvalues as the tip tension, $\bar{\sigma}$, is varied, while the deployment rate is assumed to be a constant value. Each of the three parts (a), (b), and (c) of Fig. 5 corresponds to a different value of extension rate, \dot{L} , namely 0.3, 0.5, and 0.7 m/s, respectively. Owing to the fact that a frozen study is being conducted using specific values of boom length, the results are produced using different values of L , namely 40, 60, 80, and 100 m (shown using solid, dashed, dash-dotted, and dotted lines, respectively). Similar results are presented in Fig. 6, but using a sail that features a heavier membrane, namely one with μ an order of magnitude larger than that in 5. The extension rates used in the former, namely 0.1, 0.15, and 0.2 m/s, are intentionally selected to be smaller than those in the latter, to produce similar eigenvalue patterns.

The results show interesting effects caused by changes in the sail’s pretension, deployment rate, and relative boom/membrane mass. In part (b) of both figures, the first mode experiences a vanishing of oscillation frequency. A similar effect is observed in [35], [36] and [22], where a critical value of travel rate is obtained at which the frequency becomes zero; however, unlike those works that involved fixed-length travelling continua and similar to [33] and [15] that examined extending continua of varying length, the vanishing of the imaginary component in Figs. 5 and 6 does not imply flutter instability, since the corresponding real parts are still negative. Within the confines of the range of $\bar{\sigma}$ considered in this section, namely 100 to 500 Pa, further increase in extension rate (as is done in parts (c) of both figures) is required to introduce the possibility of the system’s divergence instability, which occurs when the maximum tension drops below $\bar{\sigma} \approx 191$ Pa and $\bar{\sigma} \approx 157$ Pa for $\dot{L} = 0.7$ m/s and $\dot{L} = 0.2$ m/s with the light- and heavy-membrane sails, respectively. Mathematically, divergence is caused when the equivalent stiffness matrix in 6 loses its positive-definiteness.

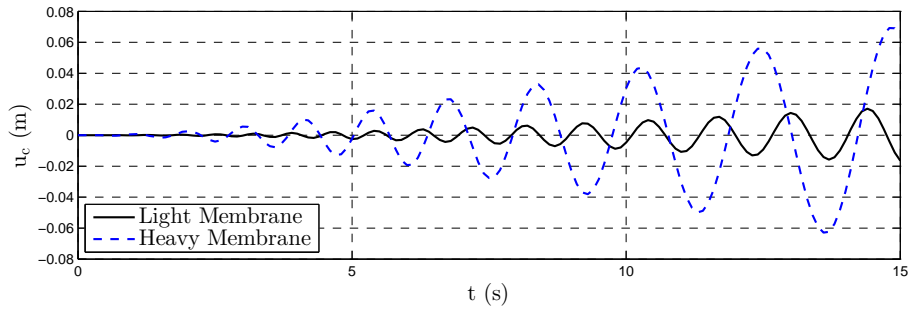
Two more observations with regards to Figs. 5 and 6 are in order: first, not all vibration modes experience divergence instability at the same time, and second, a heavier membrane seems to increase the system’s potential to suffer instability (since similar eigenvalue evolutions are obtained in the two figures, whereas the extension rates of the heavier membrane in Fig. 6 are smaller). The former observation is consistent with what was pointed out in past works on axially-translating continua, such as in [2] where fourth-order beam-like systems’ dispersive nature is recognized to be responsible for different critical speeds for each vibration mode.



(a)



(b)



(c)

Fig. 4: Simulated Sail Deployment Process with Asymmetric ICs (from $L(0) = 10$ m to $L(t_f) = 15$ m in 15 s): (a) Light Membrane with $\mu = 1.39 \times 10^{-2}$ kg/m², (b) Heavy Membrane with $\mu = 1.39 \times 10^{-1}$ kg/m², and (c) Comparison of Boom (c) Tip Deflection Histories in Both Sails

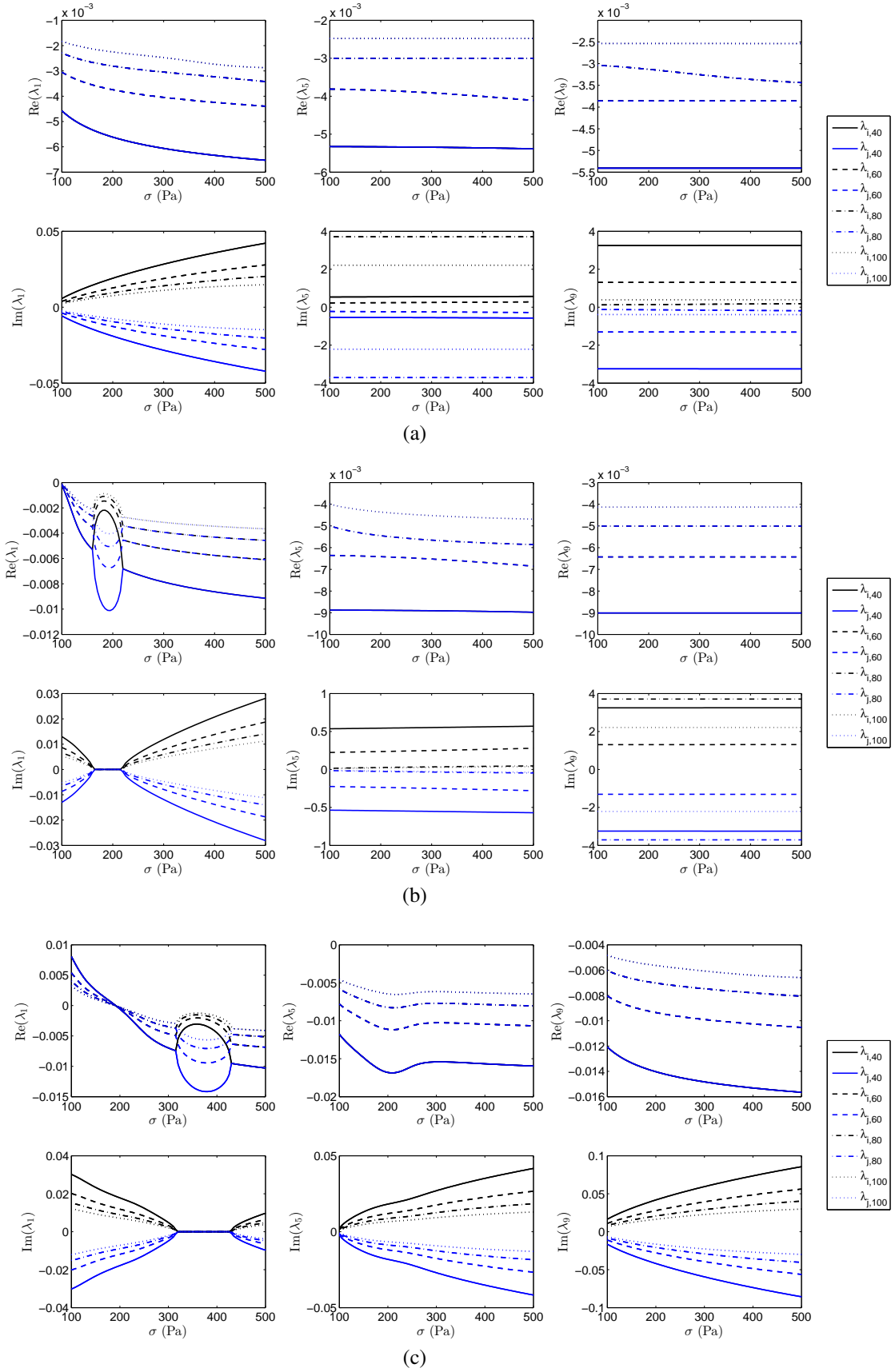


Fig. 5: Light Membrane ($\mu = 1.39 \times 10^{-2}$ kg/m²) - Real and Imaginary Parts of Pairs (Blue and Black) of Eigenvalues Corresponding to First 3 Modes vs. Pretension Magnitude, Using Various Lengths (Different Line Patterns) and Various Extension Rates: (a) $\dot{L} = 0.3$ m/s, (b) $\dot{L} = 0.5$ m/s, and (c) $\dot{L} = 0.7$ m/s

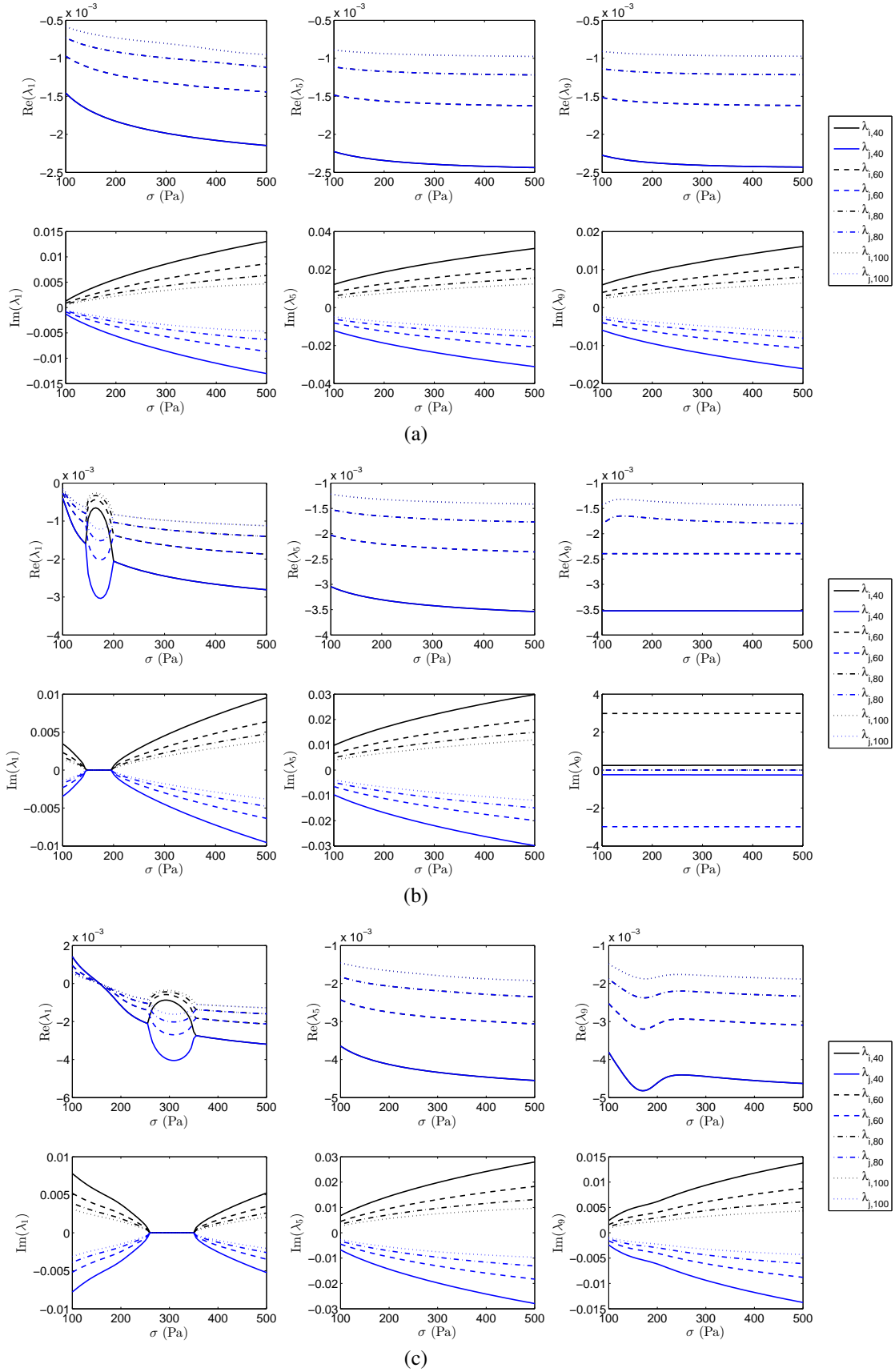


Fig. 6: Heavy Membrane ($\mu = 1.39 \times 10^{-1} \text{ kg/m}^2$) - Real and Imaginary Parts of Pairs (Blue and Black) of Eigenvalues Corresponding to First 3 Modes vs. Pretension Magnitude, Using Various Lengths (Different Line Patterns) and Various Extension Rates: (a) $\dot{L} = 0.1$ m/s, (b) $\dot{L} = 0.15$ m/s, (c) $\dot{L} = 0.2$ m/s

5 Conclusions

Inspired by and building upon an extensive body of literature on the dynamics of translating continua, this manuscript describes a methodology for and presents dynamics and stability simulation results related to the deployment of a hybrid system of moving continua, namely a multibody system of flexible beams (mathematically second-order) and thin membranes (fourth-order). The presented formulation extends that of [26] (that primarily focused on a single quadrant consisting of two booms and a membrane), and the stability analysis complements the results of that work and sheds more light on the vibrations characteristics of solar sails during their deployment.

Assuming the discretized equations of motion for a single quadrant are known (and upon providing the expressions for the associated matrices), this document details a “lifting” procedure on the matrices to enable their use in the extended system-level equations of motion. The resulting system of second-order differential equations is then recast into first-order form, and the kinetic (vibration) approach to stability is adopted by conducting an eigenvalue analysis on the resulting system. Numerical integration of the equations of motion and computation of the system’s “frozen” (at a given length) eigenvalues are performed. The modelling and simulation results are validated by comparison against constant-length modal analysis via FEM from past literature, and using a symmetric deployment scenario as a sanity check. The stability analysis results show possibility of divergence if the membrane pretension is below a threshold (which increases as the extension rate increases). Repeating the simulations using a heavier membrane suggests increased wave propagation and diminished stability properties (considering the same tension ranges as those of the lighter sail) in terms of tolerance for increased extension rates.

Acknowledgements

This research was supported by the Ontario Graduate Scholarship (OGS) program, jointly funded by the Province of Ontario and the University of Toronto.

Appendix A

To significantly improve computational efficiency, the problem was transformed in [26] from that of spatially-fixed points within time-varying boundaries, namely x and y that satisfy $0 < x < L(t)$ and $0 < y < L(t)$, to that of moving points within fixed boundaries, namely $\hat{x} \triangleq x/L(t)$ and $\hat{y} \triangleq y/L(t)$ that satisfy $0 < \hat{x}(t) < 1$ and $0 < \hat{y}(t) < 1$ (as was done in [45, 18, 46], among others). With this transformation, the following boom-related matrices were obtained in [26]:

$$\mathbf{M}_B = \rho L \int_{0^+}^1 \Psi_a \Psi_a^\top d\hat{x} \quad (10a)$$

$$\mathbf{G}_B = \rho \dot{L} \int_{0^+}^1 (1 - \hat{x}) \Psi_a \Psi_{a,\hat{x}}^\top d\hat{x} \quad (10b)$$

$$\mathbf{K}_{B,T} = \rho \frac{\dot{L}^2}{L} \int_{0^+}^1 (1 - \hat{x})^2 \Psi_{a,\hat{x}} \Psi_{a,\hat{x}}^\top d\hat{x} \quad (10c)$$

$$\mathbf{K}_{B,U} = -\frac{\bar{\sigma}A}{L_0} \int_{0^+}^1 \hat{x} \Psi_{a,\hat{x}} \Psi_{a,\hat{x}}^\top d\hat{x} + \frac{EI}{L^3} \int_{0^+}^1 \Psi_{a,\hat{x}\hat{x}} \Psi_{a,\hat{x}\hat{x}}^\top d\hat{x} \quad (10d)$$

where ρ and EI are the booms’ mass density per unit length and bending stiffness, respectively. The commas in the subscripts denote differentiation with respect to the variables that follow them. The column matrix $\Psi_a(\hat{x})$ stores the beam eigenfunctions in terms of \hat{x} , and $\Psi_{a,\hat{x}}(\hat{x}) = \Psi_{a,x}/L$ and $\Psi_{a,\hat{x}\hat{x}}(\hat{x}) = \Psi_{a,xx}/L^2$ are its spatial derivatives

with respect to \hat{x} . Since all of the integrals of Eq. (10) are only \hat{x} -dependent, numerical integration (in the absence of analytic expressions) is required only once, and not at each time-step. As another welcome consequence of the coordinate transformation, the rate matrices $\dot{\mathbf{M}}_B$ and $\dot{\mathbf{G}}_B$ are readily obtained by applying the chain rule to the coefficients outside the integrals. Note that the matrices in Eq. (10) are placed in quadrant-level augmented $n \times n$ block-diagonal form (with a $\mathbf{0}$ block corresponding to \mathbf{q}_{ab}) before their use in Eq. (4). For example, $\tilde{\mathbf{M}}_B \triangleq \text{blockdiag}\{\mathbf{M}_B, \mathbf{M}_B, \mathbf{0}_{n_M \times n_M}\}$.

Similarly, the following membrane-related matrices were obtained in [26]

$$\tilde{\mathbf{M}}_M = \mu L^2 \int_{0^+}^1 \int_{0^+}^{1-\hat{x}} \hat{\mathbf{A}} \hat{\mathbf{A}}^\top d\hat{y} d\hat{x} \quad (11a)$$

$$\tilde{\mathbf{G}}_M = \mu L \dot{L} \int_{0^+}^1 \int_{0^+}^{1-\hat{x}} \hat{\mathbf{A}} \hat{\mathbf{B}}^\top d\hat{y} d\hat{x} \quad (11b)$$

$$\tilde{\mathbf{K}}_{M,T} = \mu \dot{L}^2 \int_{0^+}^1 \int_{0^+}^{1-\hat{x}} \hat{\mathbf{B}} \hat{\mathbf{B}}^\top d\hat{y} d\hat{x} \quad (11c)$$

$$\tilde{\mathbf{K}}_{M,U} = \frac{\bar{\sigma} h L}{L_0} \int_{0^+}^1 \int_{0^+}^{1-\hat{x}} (\hat{x} + \hat{y}) \left(\hat{\mathbf{C}} \hat{\mathbf{C}}^\top + \hat{\mathbf{D}} \hat{\mathbf{D}}^\top - (\hat{\mathbf{C}} \hat{\mathbf{D}}^\top + \hat{\mathbf{D}} \hat{\mathbf{C}}^\top) \right) d\hat{y} d\hat{x} \quad (11d)$$

where μ is the membrane's mass density per unit area, and the following intermediate matrices are used:

$$\hat{\mathbf{A}} \triangleq \begin{bmatrix} \Psi_a \\ \Psi_b \\ \Phi \end{bmatrix}, \quad \hat{\mathbf{C}} \triangleq \begin{bmatrix} \Psi_{a,\hat{x}} \\ \mathbf{0} \\ \Phi_{,\hat{x}} \end{bmatrix}, \quad \hat{\mathbf{D}} \triangleq \begin{bmatrix} \mathbf{0} \\ \Psi_{b,\hat{y}} \\ \Phi_{,\hat{y}} \end{bmatrix}, \quad \hat{\mathbf{B}} \triangleq (\hat{v}_{\hat{x}} - \hat{x}) \hat{\mathbf{C}} + (\hat{v}_{\hat{y}} - \hat{y}) \hat{\mathbf{D}}$$

where $\hat{\mathbf{C}}$ and $\hat{\mathbf{D}}$ contain derivatives of the eigenfunctions with respect to \hat{x} and \hat{y} , necessitating the use of $1/L$ or $1/L^2$ factors for first and second derivatives. In addition, $\hat{v}_{\hat{x}} = v_x/L$ and $\hat{v}_{\hat{y}} = v_y/L$ (based on the velocity distribution in 1). The same comments as those made about the boom matrices regarding computational efficiency hold.

References

- [1] C. D. Mote Jr., "Dynamic stability of axially moving materials," *Shock and Vibration Digest*, vol. 4, pp. 2–11, 1972.
- [2] J. A. Wickert and C. D. Mote Jr., "Current research on the vibration and stability of axially-moving materials," *Shock and Vibration Digest*, vol. 20, no. 5, pp. 3–13, 1988.
- [3] W. D. Zhu and J. Ni, "Vibration and stability of time-dependent translating media," *Shock and Vibration Digest*, vol. 32, no. 5, pp. 369–379, Sept. 2000.
- [4] J. M. Hedgepeth, "Dynamics of a large spin-stiffened deployable paraboloidal antenna," *Journal of Spacecraft and Rockets*, vol. 7, no. 9, pp. 1043–1048, Sept. 1970.
- [5] G. J. Cloutier, "Dynamics of deployment of extendible booms from spinning space vehicles," *Journal of Spacecraft and Rockets*, vol. 5, no. 5, pp. 547–552, May 1968.
- [6] D. B. Cherkas, "Dynamics of spin-stabilized satellites during extension of long flexible booms," *Journal of Spacecraft and Rockets*, vol. 8, no. 7, pp. 802–804, July 1971.
- [7] P. C. Hughes, "Dynamics of a spin-stabilized satellite during extension of rigid booms," *C.A.S.I. Transactions*, vol. 5, no. 1, pp. 11–14, Mar. 1972.
- [8] G. F. Carrier, "The spaghetti problem," *The American Mathematical Monthly*, vol. 56, no. 10, pp. 669–672, 1949.

- [9] R. A. Sack, "Transverse oscillations in travelling strings," *British Journal of Applied Physics*, vol. 5, no. 6, pp. 224–226, 1954.
- [10] W. L. Miranker, "The wave equation in a medium in motion," *IBM Journal of Research and Development*, vol. 4, no. 1, pp. 36–42, Jan. 1960.
- [11] C. M. Leech, *The Dynamics of Beams under the Influence of Convecting Inertial Forces*. PhD thesis, University of Toronto, Toronto, ON, 1970.
- [12] B. Tabarrok, C. M. Leech, and Y. I. Kim, "On the dynamics of an axially moving beam," *Journal of the Franklin Institute*, vol. 297, no. 3, pp. 201–220, Mar. 1974.
- [13] P. K. C. Wang and J.-D. Wei, "Vibrations in a moving flexible robot arm," *Journal of Sound and Vibration*, vol. 116, no. 1, pp. 149–160, Jul. 1987.
- [14] P. K. C. Wang and J.-D. Wei, "Corrections and remarks on 'vibrations in a moving flexible robot arm'," *Journal of Sound and Vibration*, vol. 172, no. 3, pp. 413–414, May 1994.
- [15] L. H. Wang, Z. D. Hu, Z. Zhong, and J. W. Ju, "Hamiltonian dynamic analysis of an axially translating beam featuring time-variant velocity," *Acta Mechanica*, vol. 206, no. 3, pp. 149–161, 2009.
- [16] X.-D. Yang and W. Zhang, "Energetics and invariants of axially deploying beam with uniform velocity," *AIAA Journal*, vol. 54, no. 7, pp. 2181–2187, Jul. 2016.
- [17] P. C. Cherkas and D. M. Gossain, "Dynamics of a flexible solar array during deployment from a spinning spacecraft," *C.A.S.I. Transactions*, vol. 7, no. 1, pp. 10–18, Mar. 1974.
- [18] P. C. Hughes, "Deployment dynamics of the Communications Technology Satellite - a progress report," in *Proceedings of the ESRO Symposium on Dynamics and Control of Non-Rigid Spacecraft*, vol. SP 117, (Frascati, Italy), pp. 335–340, Mar. 1976.
- [19] M. S. Janković, *Deployment Dynamics of Flexible Spacecraft*. PhD thesis, University of Toronto, Toronto, ON, 1979.
- [20] J. Niemi and A. Pramila, "FEM-analysis of transverse vibrations of an axially moving membrane immersed in ideal fluid," *International Journal for Numerical Methods in Engineering*, vol. 24, pp. 2301–2313, Dec. 1987.
- [21] H. Koivurova and A. Pramila, "Nonlinear vibration of axially moving membrane by finite element method," *Computational Mechanics*, vol. 20, no. 6, pp. 573–581, Nov. 1997.
- [22] C. Shin, C. Jintai, and W. Kim, "Dynamic characteristics of the out-of-plane vibration for an axially moving membrane," *Journal of Sound and Vibration*, vol. 286, no. 4-5, pp. 573–581, Sept. 2005.
- [23] P. C. Hughes and S. C. Garg, "Dynamics of large flexible solar arrays and application to spacecraft attitude control system design," Tech. Rep. 179, University of Toronto Institute for Aerospace Studies, Toronto, ON, Feb. 1973.
- [24] F. J. Shaker, "Free-vibration characteristics of a large split-blanket solar array in a 1-g field," Tech. Rep. TN D83-7576, NASA, Washington, D. C., Dec. 1976.
- [25] G. E. Weeks, "Dynamic analysis of a deployable space structure," *Journal of Spacecraft and Rockets*, vol. 23, no. 1, pp. 102–107, 1986.
- [26] B. Vatankhahghadim and C. J. Damaren, "Deployment dynamics and stability analysis of a membrane attached to two axially-moving beams," *Journal of Sound and Vibration*, Under Review (Submitted in Jan. 2018).
- [27] W. D. Zhu and J. Ni, "Energetics and stability of translating media with an arbitrarily varying length," *Journal of Vibration and Acoustics*, vol. 122, no. 3, pp. 295–304, July 2000.
- [28] Y. Shirasawa, O. Mori, Y. Miyazaki, H. Sakamoto, M. Hasome, N. Okuizumi, H. Sawada, H. Furuya, S. Matsunaga, and M. Natori, "Analysis of membrane dynamics using multi-particle model for solar sail demonstrator 'IKAROS'," in *52nd AIAA/ASME/ASCE/AHS/ASC Structures, Structural Dynamics and Materials Conference*, (Denver, CO), Apr. 2011.
- [29] J. Zhao, Q. Tian, and H.-Y. Hu, "Deployment dynamics of a simplified spinning IKAROS solar sail via absolute coordinate based method," *Acta Mechanica Sinica*, vol. 29, no. 1, pp. 132–142, Feb. 2013.
- [30] Q. Tian, J. Zhao, C. Liu, and C. Zhou, "Dynamics of space deployable structures," in *Proceedings of the ASME 2015 International Design Engineering Technical Conferences & Computers and Information in Engineering Conference*, (Boston, MA), Aug. 2015.

- [31] H. Sakamoto, Y. Miyazaki, and O. Mori, "Transient dynamic analysis of gossamer-appendage deployment using non-linear finite element method," *Journal of Spacecraft and Rockets*, vol. 48, no. 5, pp. 881–890, Sept.-Oct. 2011.
- [32] M. Stylianou and B. Tabarrok, "Finite element analysis of an axially moving beam, part I: Time integration," *Journal of Sound and Vibration*, vol. 178, no. 4, pp. 433–453, Dec. 1994.
- [33] M. Stylianou and B. Tabarrok, "Finite element analysis of an axially moving beam, part II: Stability analysis," *Journal of Sound and Vibration*, vol. 178, no. 4, pp. 455–481, Dec. 1994.
- [34] H. Ziegler, *Principles of Structural Stability*. Birkhäuser Verlag Basel, 1977.
- [35] J. A. Wickert and C. D. Mote Jr., "Classical vibration analysis of axially moving continua," *ASME Journal of Applied Mechanics*, vol. 57, no. 3, pp. 738–744, Sept. 1990.
- [36] C. C. Lin, "Stability and vibration characteristics of axially moving plates," *International Journal of Solids and Structures*, vol. 34, no. 24, pp. 3179–3190, 1997.
- [37] J. A. Wickert and C. D. Mote Jr., "On the energetics of axially moving continua," *Journal of Acoustical Society of America*, vol. 85, no. 3, pp. 1365–1368, 1989.
- [38] S. Hassanpour and C. J. Damaren, "Linear structural dynamics and modal cost analysis for a solar sail," in *AIAA Spacecraft Structures Conference, AIAA SciTech Forum*, (Kissimmee, FL), 8-12 Jan. 2018.
- [39] F. Tisseur and K. Meerbergen, "The quadratic eigenvalue problem," *SIAM Review*, vol. 43, no. 2, pp. 235–286, Jun. 2001.
- [40] S. Hammarling, C. J. Munro, and F. Tisseur, "An algorithm for the complete solution of quadratic eigenvalue problems," *ACM Transactions on Mathematical Software*, vol. 39, no. 3, pp. 18:1–18:19, Apr. 2013.
- [41] M. C. Stylianou, *Dynamics of a Flexible Extendible Beam*. PhD thesis, University of Victoria, Victoria, BC, 1993.
- [42] L. H. Wang, Z. Hu, and Z. Zhong, "Dynamic analysis of an axially translating plate with time-variant length," *Acta Mechanica*, vol. 215, no. 1-4, pp. 9–23, Apr. 2010.
- [43] M. Choi, *Flexible Dynamics and Attitude Control of a Square Solar Sail*. PhD thesis, University of Toronto, Toronto, ON, 2015.
- [44] N. M. Newmark, "A method of computation for structural dynamics," *ASCE Journal of Engineering Mechanics Division*, vol. 85, no. 3, pp. 67–94, Jul. 1959.
- [45] S. Bergamaschi and A. Sinopoli, "On the flexural vibrations of arms with variable length: An exact solution," *Mechanics Research Communications*, vol. 10, no. 6, pp. 341–345, Nov.-Dec. 1983.
- [46] K. Behdinan and B. Tabarrok, "Dynamics of flexible sliding beams: Part II - transient response," *Journal of Sound and Vibration*, vol. 208, no. 4, pp. 541–565, 1997.